ADVANCED FUNCTIONAL MATERIALS
www.afm-journal.de

Aggregation-Induced Emission in a Flexible Phosphine Oxide and its Zn(II) Complexes—A Simple Approach to Blue Luminescent Materials

Christin Kirst, Fabian Knechtel, Manuel Gensler, David Fischermeier, Jens Petersen, Nader A. Danaf, Jonathan Tietze, Armin Wedel, Don C. Lamb,* Roland Mitrić,* and Konstantin Karaghiosoff**

Easily accessible blue-emitting materials are in the focus of ongoing research, as they still lack the efficiency and lifetime of their red and green counterparts. The new multidentate phosphine oxide ligands and two respective $ZnCl_2$ complexes presented here combine a straightforward synthesis with high yields and show interesting luminescent properties. The free ligand exhibits blue luminescence in the crystalline state, but not in amorphous films or diluted solution. In contrast, the Zn(II) complexes shows intense blue luminescence in the crystalline state as well as in amorphous thin films and in solution. Fluorescence lifetime imaging microscopy measurements show luminescence lifetimes of 3–6 ns indicative of fluorescence. By combining the experimental data with quantum chemical calculations, we propose a model where the conformation of the molecule is restricted, either via the crystal environment, aggregation, or the steric fixation by the coordinating central atom, blocking the nonradiative relaxation from the excited into the ground electronic state. However, this nonradiative relaxation is still possible in the gas phase via elongation of a P—C bond. These results may provide a general mechanism to explain the luminescence properties in a whole class of organic phosphine oxides.

1. Introduction

The search for novel organic solid-state luminescent materials is still attracting many researchers due to their promising application in lighting, flat panel displays, optical communication, etc. Currently, used materials are based on rather expensive and rare metals such as Ir(III), Pt(II), and Os(II) or large organic molecules.[1–10] Their synthesis is often tedious with low yields and is hardly scalable. Especially, blue emitting materials are still a challenge due to their low efficiency and limited lifetime compared to red and green emitting materials.[11,12] One approach that has been extensively pursued for organic light-emitting diode (OLED) applications is the use of phosphines or phosphine oxides as hosts, emitters, or ligands in luminescent metal complexes.[13–25] Used as hosts, particularly in blue phosphorescent (2nd generation) and thermally activated delayed fluorescence (TADF, 3rd generation) OLEDs, phosphine oxides stand out due to their high triplet-state energy (T_1) and charge mobility, and can improve device properties and performances.[15,26] The drawback of phosphines and phosphine oxides is their rather labile P—C bond.[27,28] Finding ways to stabilize this bond is crucial for the development of high-performance, long-lasting OLEDs. Possible options for reaching a stabilization are via complexation (limiting the degrees of freedom) and/or via exploitation of favorable packing effects in a crystal or aggregated solution. These effects, in the end, could also lead to aggregation-induced emission (AIE) and thus enhanced luminescence.[29–31]

C. Kirst, F. Knechtel, N. A. Danaf, J. Tietze, D. C. Lamb, K. Karaghiosoff
Department of Chemistry
Ludwig-Maximilians-Universität München
Butenandtstr. 5–13 (D), 81377 Munich, Germany
E-mail: d.lamb@cup.uni-muenchen.de; klk@cup.uni-muenchen.de

The ORCID identification number(s) for the author(s) of this article can be found under https://doi.org/10.1002/adfm.202212436.

DOI: 10.1002/adfm.202212436

F. Knechtel, N. A. Danaf, D. C. Lamb
Center for NanoScience (CeNS), NanoSystems Initiative Munich (NIM) and Center for Integrated Protein Science Munich (CIPSM)
Ludwig-Maximilians-Universität München
Butenandtstr. 5–13, 81377 Munich, Germany

M. Gensler, A. Wedel
Fraunhofer Institute for Applied Polymer Research
Geiselbergstr. 69, 14476 Potsdam-Golm, Germany
E-mail: armin.wedel@iap.fraunhofer.de

D. Fischermeier, J. Petersen, R. Mitrić
Institute of Physical and Theoretical Chemistry
University of Würzburg
Am Hubland, 97074 Würzburg, Germany
E-mail: roland.mitric@uni-wuerzburg.de

In the following, we present a picolyl derived phosphine oxide ligand and its neutral and ionic zinc-based complexes, which show a blue luminescence. By introduction of a methylene group between the pyridine unit and phosphorus, our ligands gain in flexibility while, at the same time, sufficient stability is provided when coordinated to a metal. This produces ligands and complexes that show interesting structural, chemical and physical properties.[32,33]

Materials based on these compounds could be a practicable, cheap, and a "green" alternative to the currently used heavy metal-based emitters. Many other research groups have reported luminescent complexes of related P,N-ligands before, which show promising results with regard to their luminescence properties.[34–43]

The synthesized ligand and complexes were characterized via single crystal X-ray diffraction, multinuclear NMR, IR, MS, and EA. Moreover, their photophysical properties were measured in solution, in solid state and in thin films. Fluorescence lifetime imaging microscopy (FLIM) measurements were conducted to gain insight into the time scale of the photoluminescence decay in the compounds. A quantitative Hirshfeld surface (HS) analysis was done to provide knowledge about the structural-property relationships, when combining the results with FLIM. In addition, quantum chemical calculations and molecular dynamics simulations were performed both in the gas phase and in the crystal to investigate the origin of the luminescence.

2. Results and Discussion

2.1. Synthesis and NMR Characterization

The synthesis of all compounds is depicted in **Scheme 1**. The preparation of the bis-substituted phosphine 1 was performed according to a route previously established by Pierre Braunstein, as this synthetic route leads to very high yields of the desired phosphine with an easy work-up.[44] The subsequent oxidation of 1 using an aqueous solution of H_2O_2 and recrystallization of the obtained solid yielding 93% of pure phosphine oxide 2. $ZnCl_2$ complexes of the phosphine oxide ligand 2 were prepared to investigate a possible stabilization of the compounds via the metal and the influence of coordination on the luminescence properties. The detailed procedures can be found in the Supporting Information. Compound 1 is a non-luminescent intermediate used for generating compounds 2–4. Compounds 2–4 were obtained as colorless powders and were purified by recrystallization.

We characterized the samples using NMR spectroscopy. From the ^{31}P NMR spectra in $CDCl_3$, chemical shifts were observed at –13.3 ppm for compound 1, 36.7 ppm for compound 2, 50.6 ppm for compound 3, and 49.5 ppm for compound 4. These values are similar to what is expected for such compounds.

2.2. Structural Characterization

The molecular structures of the synthesized compounds in the solid-state were investigated by single crystal X-ray crystallography. Crystals of 2, 3, and 4 were obtained by slow diffusion of cyclohexane into a solution of 2 in dichloromethane (DCM) or slow evaporation of acetonitrile for 3 and 4. The crystallographic data and structure refinement details as well as selected bond lengths and angles for all compounds are listed in the Figures S1–S3 and Tables S1–S5 (Supporting Information). Compound 2 forms pairs of molecules in the crystal, which are arranged as chains along the *b* axis (Figure S4, Supporting Information). In the crystal packing, compound 2 shows weak attractive hydrogen interactions[45] between oxygen and CH_2 hydrogen atoms (Figure S4, Supporting Information). The crystal structure of compound 3 is shown in Figure S2. The Zn(II) atom is coordinated in a distorted tetrahedral environment by the oxygen and nitrogen atoms of the phosphine oxide ligand. The phenyl ring is almost perpendicular to the coordinated trimethylpyridine ring (77.9(8)°). In the crystal packing of 3, there are attractive π–π stacking interactions present between

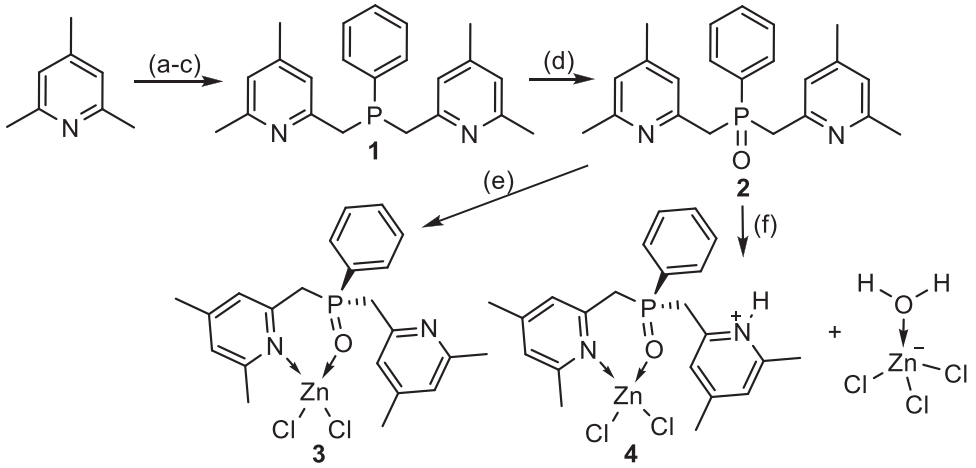

Scheme 1. Synthesis of compounds 1–4. Reactants and reaction conditions for the different steps of the synthesis: a) *n*BuLi, tetrahydrofurane, –78 °C, 1 h, b) TMSCl 2 eq, –78 °C to RT, 12 h, c) $PhPCl_2$ 0.5 eq, tetrahydrofurane, –10 °C to RT, 12 h, quantitative, d) H_2O_2, H_2O, dichloromethane, –10 °C to RT, 5 h, 93%, e), $ZnCl_2$, acetonitrile, 4 h, 97%, f) $ZnCl_2$, H_2O, HCl, acetonitrile, 4 h, 83%.

the non-coordinated trimethylpyridine rings of neighboring molecules (Figure S5, Supporting Information). Figure S3 (Supporting Information) depicts the crystal structure of compound 4 containing a protonated phosphine oxide ligand coordinating to $ZnCl_2$ and a $[Zn(H_2O)Cl_3]^-$ anion. Both Zn(II) atoms display a distorted tetrahedral environment, formed by oxygen and nitrogen atoms in the case of the cation and by three chlorine atoms and a water molecule in the case of the anion (see also Figure S6, Supporting Information).

It is known from similar picolylphosphine oxide complexes that the presented ligands are fairly flexible in solution.[32] To investigate possible structural changes of the complexes, variable temperature NMR was conducted on compounds 3 and 4 in CD_2Cl_2 (Figures S7 and S8, Supporting Information). The results show that, at room temperature, a fast dynamics is present in compound 3, where the zinc(II) atom stays coordinated to oxygen but the N-coordination switches between one collidinyl substituent and the other. This rapid exchange is drastically slowed down at low temperature. The signals for both collidinyl substituents (coordinating and non-coordinating to Zn(II)) are then visible in the ^{1}H NMR spectrum of compound 3 at –80 °C (Figure S7, Supporting Information). For compound 4, a dynamical behavior in solution is also observed, displaying only one set of signals for the collidinyl substituents (Figure S8, Supporting Information). However, when lowering the temperature to –60 °C, the dynamics is slowed down and signals for the four different methyl groups become visible in the ^{1}H NMR spectrum. Additionally, at –80 °C, reversible aggregation of compound 4 occurs, visible by a broadening of the signals in the ^{1}H NMR spectrum.

2.3. Photophysical Characterization

Solid compounds 2–4 show luminescence when illuminated with UV-light (366 nm) and in concentrated solution when illuminated at 254 nm. When diluted in solution, neither the ligand 2 nor the complexes 3–4 show any luminescence, which could implicate AIE. To gain more insights into the luminescent properties of the compounds, a thorough photophysical characterization was performed.

The luminescent properties of compounds 2–4 were investigated in solution (acetonitrile), in powder form (small crystals), and in spin-coated thin films (amorphous). Solutions and thin films were measured by UV–vis spectroscopy in transmission mode and luminescence spectroscopy in reflective mode using quartz glass cuvettes and substrates. Powder samples were encapsulated in a borosilicate cavity glass and measured in an Ulbricht sphere with tunable excitation wavelength and a luminescence detector attached.

Compound 2 exhibits the same absorbance behavior in solution and in thin film with two maxima at 265–266 and 271–272 nm, respectively (**Figure 1**). Illuminating the concentrated solution (10 g L^{-1}) or the freshly crystallized powder at 265 or 270 nm yields a broad luminescence in the UV to blue range from 300 to 550 nm. No significant emission is measured

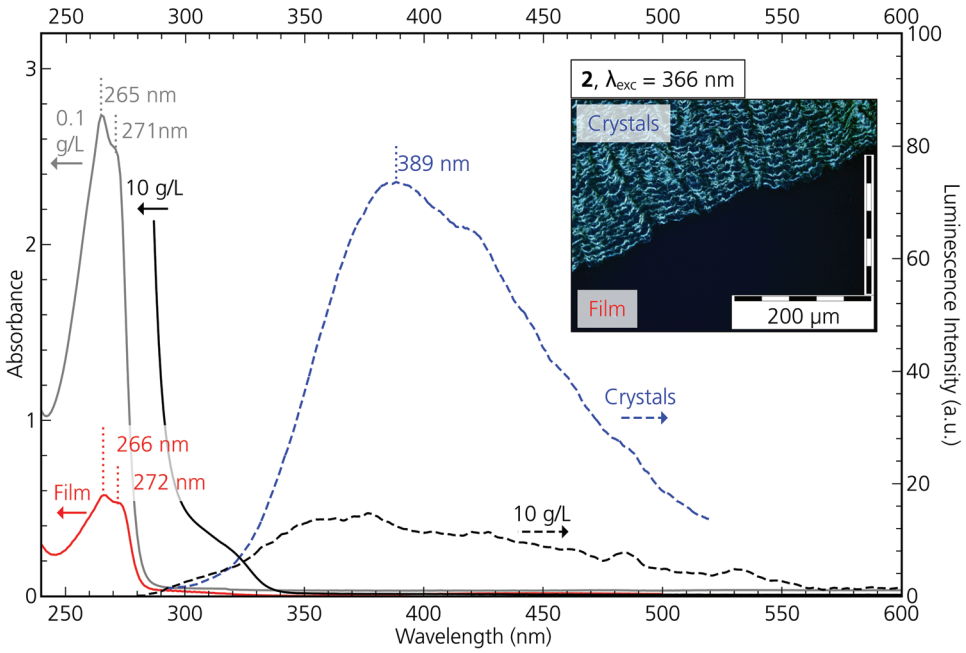

Figure 1. Luminescence properties of compound 2. The absorbance spectra were recorded from a solution of compound 2 in MeCN (grey: 0.1 g L^{-1}, black: 10 g L^{-1}) and from a thin film on quartz glass (red). The black absorbance line saturates <280 nm. Emission spectra were recorded from solution (black dashed line: 10 g L^{-1}) and a thin layer of crystals on quartz glass (blue dashed line) at an excitation wavelength of 265 nm (solution) or 270 nm (powder). The 0.1 g L^{-1} solution and thin film did not exhibit any fluorescence signal. The inset shows a microscopic color image of the luminescence from a partially crystallized thin film (top: crystallized, bottom (dark): still amorphous) with illumination at 366 nm. and thin film did not exhibit any fluorescence signal. The inset shows a microscopic color image of the luminescence from a partially crystallized thin film (top: crystallized, bottom (dark): still amorphous) with illumination at 366 nm.

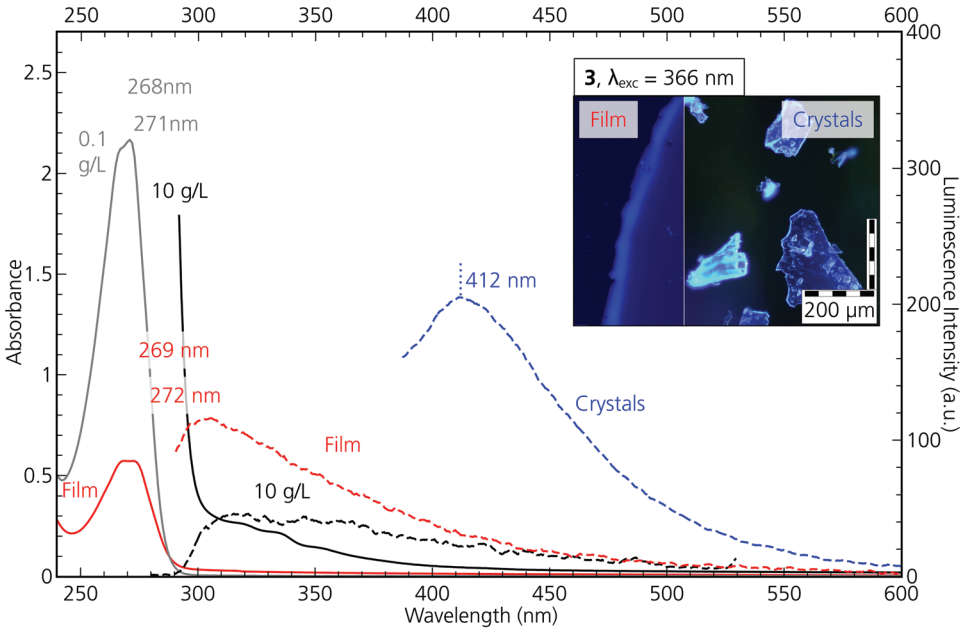

Figure 2. Luminescence properties of compound 3. The absorbance spectra were recorded from a solution of compound 3 in MeCN (grey: 0.1 g L^{-1}, black: 10 g L^{-1}) and a thin film on quartz glass (red). Emission spectra were recorded from solution (black dashed line: 10 g L^{-1}), a thin film and from a powder sample inside a borosilicate cavity glass at excitation wavelengths of 265, 270, and 350 nm, respectively. The inset shows a microscopic color image of the luminescence from the edge of a film droplet (left) and a powder sample (right) with illumination at 366 nm.

for freshly prepared thin films or thin solutions of 0.1 g L^{-1}. Interestingly, also the thin spin-coated films of compound 2 are crystallizing within some days, yielding luminescent crystals (inset in Figure 1), whose luminance is decaying over the course of several days for samples stored under air in the dark.

Complex 3 exhibits similar absorbance maxima as compound 2 (**Figure 2**). Illuminating the concentrated solution (10 g L^{-1}) or the spin-coated thin film at 265 or 270 nm yields a broad luminescence from 290 to 500 nm. The luminescence of the powder sample is measured at an illumination wavelength

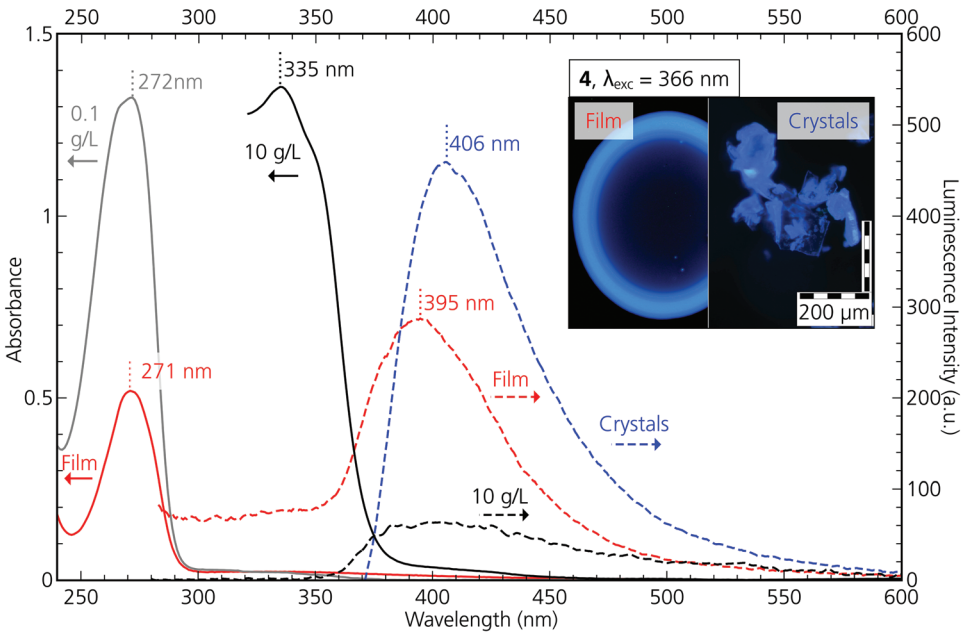

Figure 3. Luminescence properties of compound 4. The absorbance spectra were recorded from a solution of compound 4 in MeCN (grey: 0.1 g L^{-1}, black: 10 g L^{-1}) and from a thin film on quartz glass. The emission spectra were recorded from a solution (black dashed line: 10 g L^{-1}), a thin film on quartz glass (red dashed line) and from a powder sample inside a borosilicate glass cavity (blue dashed line) at excitation wavelengths of 265, 270, and 350 nm, respectively. The inset shows light microscopic color images of an amorphous droplet (left) and crystals (right) using 366 nm excitation.

of 350 nm instead of 270 nm due to the sample holder being non-transparent in the UV-range (borosilicate glass). A broad luminescence in the blue range between 380 and 550 nm was measured. Using an Ulbricht sphere setup, photoluminescence quantum yields (PLQY) of 36 ± 5% for the crystals and of 3 ± 1% for the thin film were measured. The borosilicate glass sample holder is required because, in contrast to compound 2, compound 3 does not crystallize on a quartz slide with good adhesion.

Compound 4 exhibits the same absorbance maximum as compounds 2 and 3 (**Figure 3**). Illuminating the concentrated solution (10 g L^{-1}) or the spin-coated thin film at 265 or 270 nm yields a luminescence from 360 to 500 nm. The luminescence of the powder sample measured at an illumination wavelength of 350 nm yields a broad luminescence in the blue range between 370 and 550 nm. Using an Ulbricht sphere setup, PLQY of 42 ± 1% for the crystals and of 8 ± 1% for the thin film were measured, both larger than for compound 3.

2.4. Lifetime Characterization

Fluorescence-lifetime imaging microscopy was used to measure the autofluorescence lifetime decay of compounds 2, 3, and 4. For these measurements, saturated solutions of compounds 2 and 3 were prepared in acetonitrile and of compound 4 in ethyl acetate, due to its high solubility in acetonitrile causing an increased luminescent background. Evaluation of the FLIM images shows that the samples have crystalline morphology (as for the powder samples) and different photoluminescence lifetimes (**Figure 4**; Figures S14–S16, Supporting Information). Lifetimes in the range of 3.5 to 5.9 ns were measured, which are indicative of fluorescence. Compound 2 shows spherically shaped aggregates with an average autofluorescence lifetime of ≈5.9 ns. Compound 3 forms needle-like crystals with differing lifetimes in the center (3–4 ns) and the edges (4–5 ns) of the crystals. Compound 4 displays plates of rectangular shapes with a homogeneous lifetime distribution of 3.5 ns. Figure 4b,c shows the FLIM-data analysis performed by fitting of the time-correlated single photon counting (TCSPC) histograms to exponential functions (Figure 4b; Figures S17–S19 and Table S6, Supporting Information) and by the phasor approach (Figure 4c; Figures S14–S16, Supporting Information). The phasor approach graphically transforms the fluorescence lifetime into Fourier space.[46,47] Mono-exponential lifetime decays lie along a semi-circle with a radius of 0.5 (Figure 4c, dashed black line). Long-lifetime species are located close to the origin (0, 0) and short-lifetime species near (1, 0). Multi-exponential decays lead to a weighted vector sum of the single species phasors, meaning the population lies on a straight line connecting the phasors of the pure species.[46] As a result, in the case of multi-exponential decays, the phasor falls inside the semicircle.[46,48] The phasors built up from the individual pixels of the images for of crystals 3 and 4 lie inside the arc, indicating a multi-exponential decay. For compound 2, the major population of pixels (higher occurrence) from the image exhibit a lifetime located close to the semicircle line of the phasor plot indicating a mono-exponential lifetime of 5.9 ns. A small population of the pixels is located inside the semicircle exhibiting a bi-exponential decay (Figures S14 and S17, Supporting Information).

Comparing the autofluorescence lifetime decays of the different compounds, the lifetime is reduced by coordination to $ZnCl_2$ (from 5.9 ns in 2 to ≈3.6 ns in 3 and 4). In contrast, the fluorescence intensity measured within the confocal volume increases from 332 kHz in 2 to 590 kHz in 4.

2.5. Combination of Hirshfeld Surface Analysis with the FLIM Results

As is known from previous results, morphology, crystal packing as well as intermolecular interactions play an important role in the length and uniformity of the autofluorescence lifetime decay as well as the overall fluorescence intensity.[49] The Hirshfeld surface analysis quantifies intermolecular interactions between molecules or predefined units in a crystal based on the crystallographic output file (.cif) obtained from single crystal X-ray diffraction using the software CrystalExplorer17 (see Figure S20, Supporting Information).[50,51] By combining FLIM results with the HS analysis, a correlation between intermolecular bonding interactions and fluorescence properties can be investigated.

Major contributors to the total HS are C—H···H—C and C—H···C contacts, which make up the majority of all interactions in all investigated compounds (2: 86.3%, 3: 67.1%, and 4: 50.4%). The π–π stacking interactions are almost non-existent in compound 2 (C···C: 0% and C···N: 0.6%) and 4 (C···C: 0.3% and C···N: 0%), and only increase slightly in 3 (C···C: 1.3% and C···N: 0.9%). The C—H···N, C—H···Cl, and C—H···O contacts represent the attractive, non-classical hydrogen bonds and contribute with 13.2% to the HS of compound 2, 30.4% in 3, and 48.2% in 4. The relative amount of C—H···N and C—H···O contact contributions decreases with coordination to the Zn(II), as expected.

By combining the FLIM results with the HS analysis, we demonstrated previously that the increase in the attractive hydrogen bond interactions within crystals of picolyl derived phosphine compounds can result in an increase in the fluorescence intensity.[49] This might be explained by increased rigidification of the molecule, which influences both the transition dipole moment and the non-radiative decay rates. In the case of the π–π stacking interactions, the compounds here follow a clear trend: the higher the π–π stacking content, the lower the intensity (**Figure 5**a). Compound 4 has the least amount of π–π stacking interactions and additionally shows the highest intensity and shortest fluorescence lifetime of the three compounds. As an increase in π–π interactions usually leads to reduced fluorescence intensity, this trend is to be expected. However, as those interactions are minimal compared to the much more pronounced hydrogen bonding interactions for all investigated compounds, their influence on the fluorescence intensity should be insignificant.

Regarding the fluorescence lifetime, a clear decrease is observed with an increasing amount of attractive hydrogen bonding (Figure 5b), which has been observed for other systems as well.[52] As reported previously,[49] we also observed the shorter fluorescence lifetimes for the brightest species (Figure 5c). Additional effects apart from the types of hydrogen

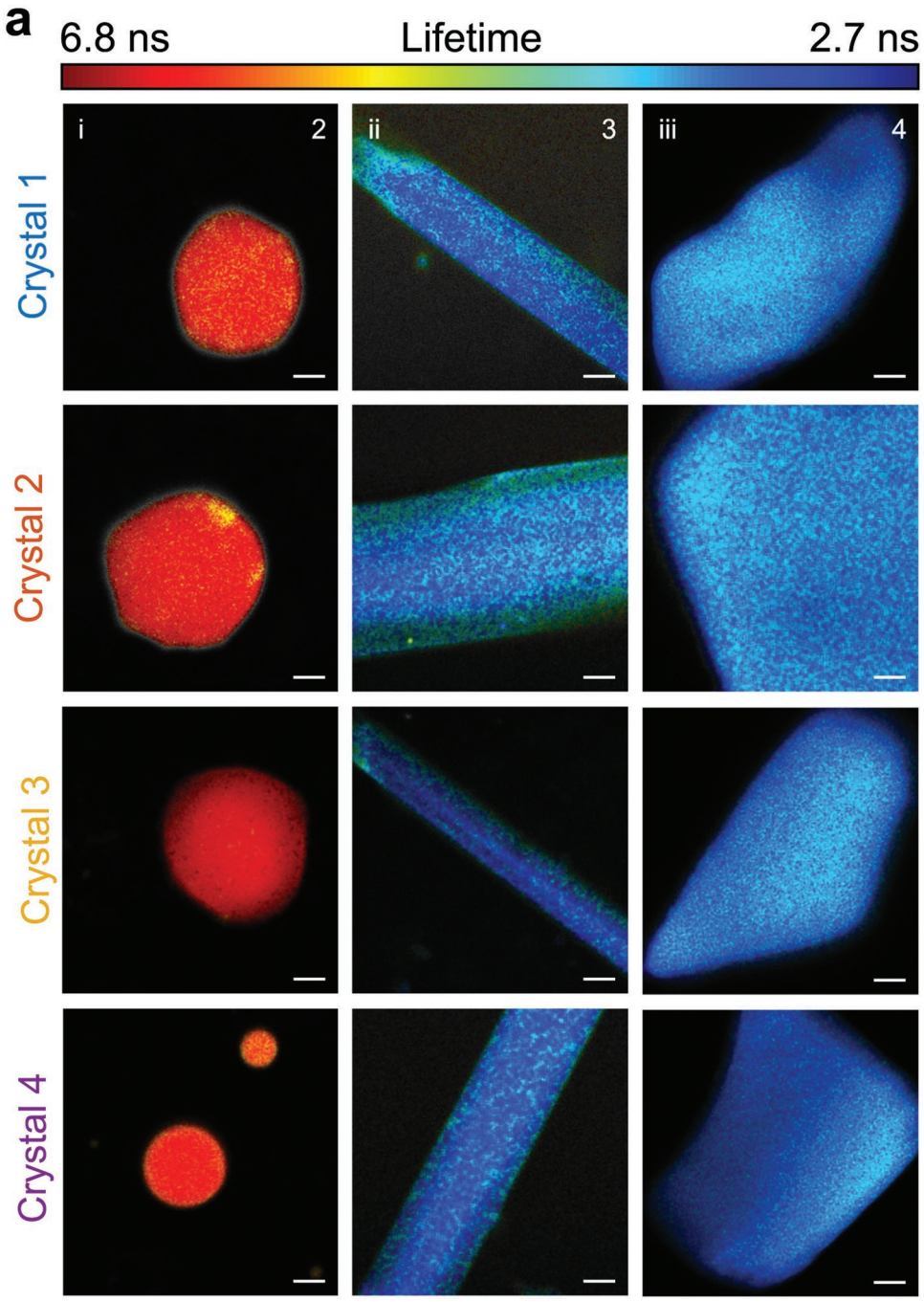

Figure 4. FLIM images and fluorescence lifetime decays of the compounds 2 (left column, i, scale bars 1 µm), 3 (middle column, ii, scale bars 4 µm), and 4 (right column, iii, scale bars 3 µm) highlighting their diverse structural morphologies. a) FLIM images of representative crystals for the three compounds. The color code indicates the fluorescence lifetime as a function of the spatial position on the crystal. The color legend is shown in the upper panel. b) The fluorescence lifetime decay for each crystal shown in a). c) Phasor plot of the four FLIM images per compound as shown in a), determined by phasor transformation of the individual lifetimes for each spatial pixel in the image of the crystals. The grey line (plotted in all three panels) was determined from the sum of all FLIM images to provide an axis for calculating the fluorescence lifetime color bar. Insets: The color bar in the phasor plots represents the number of pixels exhibiting the particular phasor value (blue indicating the lowest and red indicating the highest occurrence).

bonds and crystal density influence the intensity values in these compounds. The coordination to the metal leads to a lower lifetime of the fluorescence (compound 2 vs 3 and 4) and, of the metal containing molecules, the ionic compound (compound 4) has a higher intensity compared to compound 3 (Figure 5c).

2.6. Quantum Chemical Calculations and Nonadiabatic Dynamics Simulations

To shed light on the different emission behavior in the crystalline, amorphous thin film and solution phases and to explain

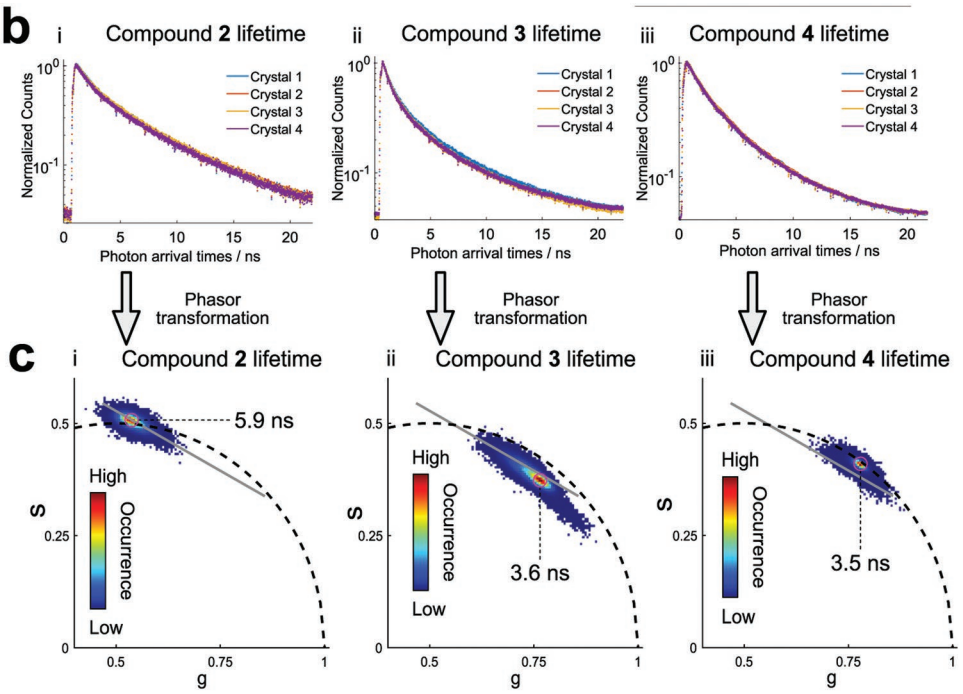

Figure 4. Continued.

the origin of the observed photoluminescence, quantum chemical calculations and nonadiabatic surface-hopping simulations of the coupled electron-nuclear dynamics were performed. A detailed description of the employed methods can be found in the Section 1.9 (Supporting Information).

The dynamical behavior of compound 2 in isolated form as well as in the crystal environment was simulated starting in the first excited singlet state. Of the ten gas-phase trajectories of the isolated compound propagated at 300 K, four decayed to the electronic ground state within 2.5 ps via a conical intersection (CI). In most of these cases, the involved CI was characterized by an increased C—P bond length (up to 2.8 Å), as illustrated in **Figure 6**. This configuration seems to be stabilized by a π–π interaction of one collidine and the benzene ring, which assume a nearly parallel stacking-type configuration when reaching the CI. Access to the CI is limited by an energy barrier, which can be overcome thermally. This is further confirmed by trajectories propagated at an elevated temperature of 400 K, where three trajectories out of five decay via elongation of the C—P bond. These results indicate what might happen in diluted solution and thin films, where the molecular environment may be flexible enough to allow for molecular motions similar to those in the gas phase.

In contrast, in the crystal phase, steric hindrance from the neighboring molecules leads to a different behavior, as becomes evident from our nonadiabatic dynamics simulations for two crystal models of compound 2. These were constructed using a quantum mechanical-molecular mechanical (QM/MM) approach, where a single molecule was described quantum mechanically (QM part) while the crystal environment of several 100 molecules was represented by a classical force field (MM part). Specifically, six trajectories were run with all MM molecules subjected to rigidifying constraints, while an additional 11 trajectories were propagated with an inner layer of 14 molecules allowed to move unconstrained (Section 1.9, Supporting Information). Relaxation to the ground state was not observed for any of these trajectories within the propagation time of 3 ps. This indicates that the frustrated and densely packed crystal environment hinders access to the conical intersections, which is a frequently observed principle for many systems showing AIE.[53–55]

The outcome of these dynamics simulations hints at the presence of a nonradiative relaxation channel on the picosecond time scale for compound 2 in the gas phase, which is blocked in the crystal phase. Given the typical nanosecond time scale of fluorescence, which has been also established for the molecules discussed here (see Section 2.5 above), the gas phase fluorescence emission should be improbable due to the competition with the much faster nonradiative relaxation.

To elucidate the nature of the actual measured photoluminescence, excitation energies between the energy-optimized geometries of the ground and excited electronic states (adiabatic energies), vibrationally resolved fluorescence and phosphorescence spectra, as well as radiative lifetimes were calculated for compound 2 in the gas phase. As described in detail in the (Section 8, Supporting Information), a singlet excited state of $n\pi^*$ character (similar to the one found in isolated pyridine[56,57]) as well as one involving excitation from an oxygen lone pair p-orbital to π^* orbitals of the ring systems were found (Figure S22 and Table S9, Supporting Information). These correspond to vertical emission energies of 3.76 and 2.15 eV, respectively. For the lowest triplet state, a vertical emission energy of 3.11 eV was obtained.

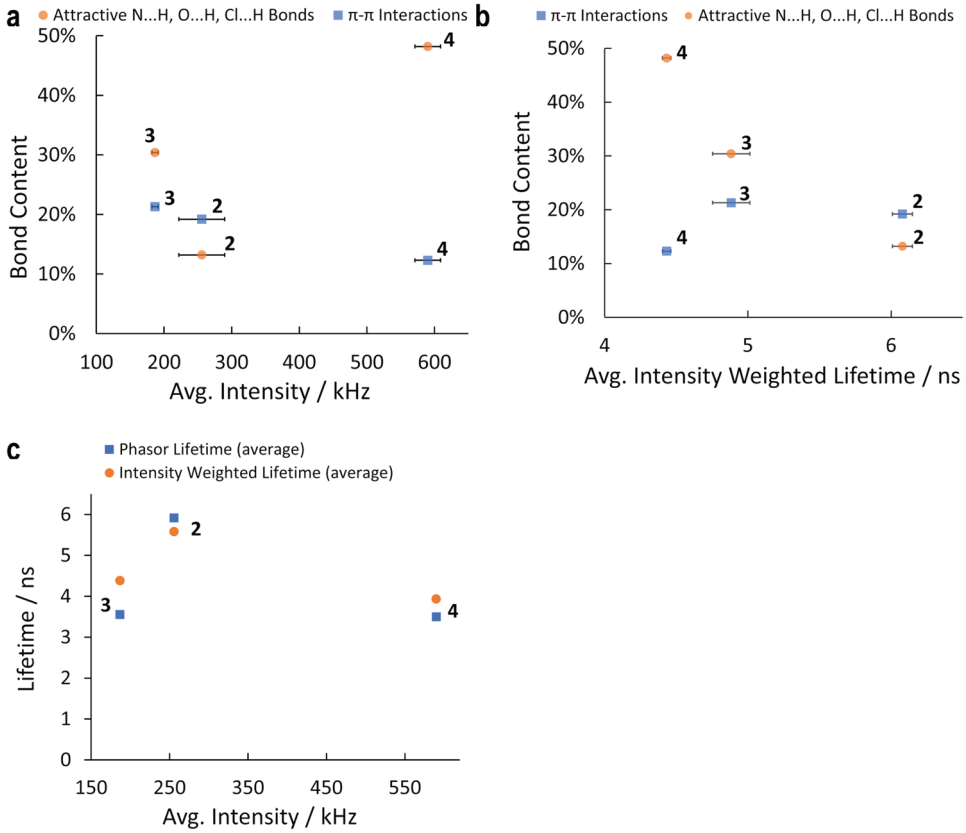

Figure 5. The relationship between fluorescence lifetime and intensity relative to the attractive bond contents for the three compounds imaged in Figure 4. a) The correlation of the average fluorescence intensity with respect to the attractive bond content for the investigated solid-state molecular structures of the respective compounds. b) The correlation between the average intensity weighted fluorescence lifetimes with respect to the bond content. c) The correlation of the average fluorescence intensity with respect to the average intensity weighted lifetime.

For the nπ^* state as well as for the lowest triplet state, emission spectra and lifetimes could be calculated (Figures S24–S26 and Table S12, Supporting Information). Overall, the obtained intensity for fluorescence is about nine orders of magnitude higher than for phosphorescence (see Figures S24–S26, Supporting Information), which is paralleled by lifetimes of ≈2 ns for fluorescence versus 1.6 s for phosphorescence (see the rate constants in the Table S12, Supporting Information). The calculated emission maximum of the fluorescence from the nπ^* state is situated at 320 nm, which fits well to the experimentally known fluorescence of the isolated pyridine chromophore.[58] However, fluorescence of the latter is very weak due to the nπ^* state having a very low oscillator strength, and this situation is similar in compound 2 (cf., Table S9, Supporting Information), making it improbable that the measured intense fluorescence originates from the nπ^* state. This assumption is corroborated by the fact that the experimentally found emission maximum of compound 2 lies at much larger wavelengths (367 nm in solution, 389 nm in the crystalline phase), indicating that another state should be responsible for emission. A candidate for this might be the lone pair-π^* state, which has a higher oscillator strength than the nπ^* state at the respective optimized excited state geometry (cf., Table S9, Supporting Information). Although its excitation energy at this geometry is too low in the gas phase (2.15 eV, cf. Figure S22, Supporting Information), it might be higher in the condensed phase, where the more rigid environment prevents strong structural deformations and thus the lowering of the excitation energy.

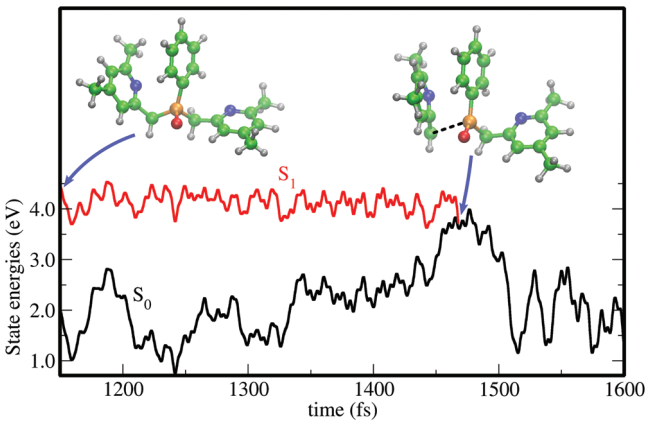

Figure 6. Final stage of the excited state dynamics of compound 2 along a simulated surface-hopping trajectory. The time evolution of the electronic state energies is shown for a temporal range between ≈ 1150 and 1600 fs after initialization of the trajectory. At t = 1468 fs, the transition to the ground state occurs via a conical intersection characterized by an elongated C—P bond (dashed line). The insets show the molecular structures at the conical intersection and at the first time-step of the presented cutout (1150 fs).

To substantiate this hypothesis, the excited state character and approximate fluorescence intensities were calculated for the geometries observed along the crystal trajectories of compound 2. Indeed, the excited state character is dominated by the lone pair-π^* excitation, and the fluorescence spectrum shown in Figure S26 (Supporting Information) exhibits a maximum ≈430 nm, which is in fair agreement with the experimental spectrum shown in Figure 1. Although the calculated phosphorescence from the lowest triplet state also has a maximum in this wavelength range (see Figure S25, Supporting Information), the presence of a nearby singlet state as well as the very long calculated phosphorescence lifetime contrasting with the ns timescale obtained in the FLIM experiments support the conclusion that the experimentally observed emission is indeed due to fluorescence.

For compound 3, the low-lying excited states are summarized in the Figure S23 and Table S10 (Supporting Information). An excited singlet-state of nπ^* character similar to the case of compound 2 could be found, exhibiting an adiabatic excitation energy of 4.67 eV. The vertical energy difference to the ground state at the optimized excited state geometry, which is a rough estimate of the position of the fluorescence maximum, amounts to 3.88 eV (320 nm). This matches well with the onset of the experimental emission spectrum in the amorphous phase with a luminescence maximum at 303 nm. The measured PLQY for this emission is only 3% (cf. Section 2.4), which is consistent with a weakly allowed nπ^* state.

In addition, also an excited singlet-state of lone pair-π^* character has been found—however, this time, involving the lone pairs of the chlorine atoms. Due to a strongly deviating geometry of this state compared to the ground state, no fluorescence spectrum could be calculated, and the vertical energy difference to the ground state in the excited state geometry is very low. The calculated phosphorescence spectrum from the lowest-lying triplet state, in contrast, is peaked at 430 nm (Figure S27, Supporting Information) and appears to match the measured luminescence maximum at 412 nm for the crystalline compound (Figure 2). However, as for compound 2, a small intensity and long time-constant (0.6 s; Table S12, Supporting Information) were calculated, while the FLIM measurements yield a nanosecond timescale for emission. This indicates that, by a similar reasoning as for compound 2, fluorescence emission should be more likely than phosphorescence also for compound 3, and that the fluorescence in the crystal might be due to the lone pair-π^* state when its geometry is less distorted in the crystal than in the gas phase.

3. Conclusion

We have presented a novel, functionalized phosphine oxide ligand and its $ZnCl_2$ complexes that show an unexpected but interesting and fascinating blue luminescence. The synthesis of these compounds is straightforward, efficient and scalable starting from commercially available and inexpensive reactants. The resulting compounds were characterized using NMR, MS, IR spectroscopy, EA, and X-ray crystallography. Variable temperature NMR measurements revealed that both complexes show a dynamic behavior in solution. However, the dynamics is minimized in compound 4, where the nitrogen atom of the second collidinyl ring is protonated. The characterization of the physical properties of the compounds in solid/crystalline-state, solution and thin films was performed by absorption and fluorescence excitation/emission spectroscopy. The emission maxima of all compounds are ≈400 nm, indicating a possible use as blue emitters. Complexes 3 and 4 form stable thin films. However, only compound 4 exhibits significant luminescence in the thin film. The PLQY for powdered samples of compounds 3 and 4 are both ≈40% when excited at 350 nm, which is comparable to other known, blue luminescent Zn(II) complexes. FLIM measurements reveal luminescent lifetimes of 3.5–5.9 ns, with compound 2 having the longest lifetime, but compound 4 displaying the highest luminescence intensity. By combining these results with the Hirshfeld surface analysis, we further conclude that higher π–π stacking interactions seem to correlate with lower luminescence intensity, and low fluorescence lifetimes seem to correlate with high amounts of attractive hydrogen bonding. Additional effects such as coordination, charge of the molecule, the type of hydrogen bonds, and crystal density most likely also influence both the luminescence intensity and fluorescence lifetimes.

Quantum chemical calculations and nonadiabatic dynamics simulations were used to elucidate the nature of the luminescence exhibited in the solid state as well as the non-radiative relaxation pathways in the gas phase. We propose a model in which the crystal environment, aggregation, and/or the steric fixation by the coordinating central atoms blocks the thermal relaxation into the ground state, thus enabling luminescence or AIE.

All in all, these findings are not only beneficial for the ligands investigated here but are also important for similar compounds. This may open the door for a targeted refinement of phosphine ligands to obtain suitable luminescent materials for multiple possible uses in the future.

Supporting Information

Supporting Information is available from the Wiley Online Library or from the author.

Acknowledgements

C.K., F.K., M.G., and D.F. contributed equally to this work. This work was financially supported by the German Federal Ministry for Economic Affairs and Energy on the basis of a decision by the German Bundestag (ZIM, grant ZF4477702SL7, ZF4065408SL7) was gratefully acknowledged. D.C.L thankfully acknowledges the financial support of the Deutsche Forschungsgemeinschaft (DFG, German Research Foundation)–Project-ID 201269156–SFB 1032 Project B03 and Project-ID 470576387. Furthermore, this work was financially supported by the Ludwig–Maximilians–Universität München via the Department of Chemistry, the Center for NanoScience (CeNS) and the LMUinnovativ initiative BioImaging Network (BIN). A portion of this work was funded by the Federal Ministry of Education and Research (BMBF) and the Free State of Bavaria under the Excellence Strategy of the Federal Government and the Länder through the ONE MUNICH Project Munich Multiscale Biofabrication to D.C.L. Prof. Dr. T. M. Klapötke was thanked for his continuous support over the years. Furthermore, the authors thank Nathalie Robel and Jiyong Kim for their support in performing luminescence measurements.

Open access funding enabled and organized by Projekt DEAL.

Conflict of Interest

The authors declare no conflict of interest.

Data Availability Statement

The data that support the findings of this study are available in the supplementary material of this article.

Keywords

AIE, FLIM, phosphine oxide, Zn complex

Received: October 26, 2022
Revised: December 23, 2022
Published online: January 24, 2023

[1] H. Yersin, *Highly Efficient OLEDs with Phosphorescent Materials*, Wiley, NJ **2007**.
[2] H. Yersin, A. F. Rausch, R. Czerwieniec, T. Hofbeck, T. Fischer, *Coord. Chem. Rev.* **2011**, *255*, 2622.
[3] C. Adachi, M. A. Baldo, M. E. Thompson, S. R. Forrest, *J. Appl. Phys.* **2001**, *90*, 5048.
[4] D. F. O'Brien, M. a. Baldo, M. E. Thompson, S. R. Forrest, *Appl. Phys. Lett.* **1999**, *74*, 442.
[5] C.-M. Che, C.-C. Kwok, S.-W. Lai, A. F. Rausch, W. J. Finkenzeller, N. Zhu, H. Yersin, *Chem. – Eur. J.* **2010**, *16*, 233.
[6] J. Zhao, F. Dang, Z. Feng, B. Liu, X. Yang, Y. Wu, G. Zhou, Z. Wu, W.-Y. Wong, *Chem. Commun.* **2017**, *53*, 7581.
[7] C. Cebrián, M. Mauro, *Beilstein J. Org. Chem.* **2018**, *14*, 1459.
[8] T. C. Lee, J. Y. Hung, Y. Chi, Y. M. Cheng, G. H. Lee, P. T. Chou, C. C. Chen, C. H. Chang, C. C. Wu, *Adv. Funct. Mater.* **2009**, *19*, 2639.
[9] W.-C. Chen, C.-S. Lee, Q.-X. Tong, *J. Mater. Chem. C* **2015**, *3*, 10957.
[10] C.-Y. Chan, M. Tanaka, Y.-T. Lee, Y.-W. Wong, H. Nakanotani, T. Hatakeyama, C. Adachi, *Nat. Photonics* **2021**, *203*, 203.
[11] J. H. Lee, C. H. Chen, P. H. Lee, H. Y. Lin, M. K. Leung, T. L. Chiu, C. F. Lin, *J. Mater. Chem. C* **2019**, *7*, 5874.
[12] G. Hong, X. Gan, C. Leonhardt, Z. Zhang, J. Seibert, J. M. Busch, S. Bräse, *Adv. Mater.* **2021**, *33*, 2005630.
[13] C. Han, Y. Zhao, H. Xu, J. Chen, Z. Deng, D. Ma, Q. Li, P. Yan, *Chem. – Eur. J.* **2011**, *17*, 5800.
[14] U. k. Kim, J. Wong, Y. M. , S. Kumar, O. G. Hayes, F. Duncan, C.-Y. Chan, B. Y.-W. Wong, H. Ye, L.-S. Cui, H. Nakanotani, E. Zysman-Colman, C Adachi, *Chem. Lett.* **2019**, *48*, 1225.
[15] G. Mallesham, C. Swetha, S. Niveditha, M. E. Mohanty, N. J. Babu, A. Kumar, K. Bhanuprakash, V. J. Rao, *J. Mater. Chem. C* **2015**, *3*, 1208.
[16] K. Duan, D. Wang, M. Yang, Z. Liu, C. Wang, T. Tsuboi, C. Deng, Q. Zhang, *ACS Appl. Mater. Interfaces* **2020**, *12*, 30591.
[17] C. Kerzig, X. Guo, O. S. Wenger, *J. Am. Chem. Soc.* **2019**, *141*, 2122.
[18] X. Song, H. Xu, *J. Inf. Disp.* **2020**, *149*, 1.
[19] C. Han, H. Xu, *Chin. Sci. Bull.* **2019**, *64*, 663.
[20] D. Joly, P.-A. Bouit, M. Hissler, *J. Mater. Chem. C* **2016**, *4*, 3686.
[21] K. Katagiri, Y. Yamamoto, Y. Takahata, R. Kishibe, N. Fujimoto, *Tetrahedron Lett.* **2019**, *60*, 2026.
[22] M. K. Rong, F. Holtrop, J. C. Slootweg, K. Lammertsma, *Coord. Chem. Rev.* **2019**, *382*, 57.
[23] A. V. Artem'ev, M. Z. Shafikov, A. Schinabeck, O. V. Antonova, A. S. Berezin, I. Y. Bagryanskaya, P. E. Plusnin, H. Yersin, *Inorg. Chem. Front.* **2019**, *6*, 3168.
[24] C. Poriel, J. Rault-Berthelot, *Adv. Funct. Mater.* **2021**, *31*, 2010547.
[25] A. Y. Baranov, S. O. Slavova, A. S. Berezin, S. K. Petrovskii, D. G. Samsonenko, I. Y. Bagryanskaya, V. P. Fedin, E. V. Grachova, A. V Artem'ev, *Inorg. Chem.* **2022**, *61*, 10925.
[26] J. Zhang, D. Ding, Y. Wei, H. Xu, *Chem. Sci.* **2016**, *7*, 2870.
[27] N. Lin, J. Qiao, L. Duan, H. Li, L. Wang, Y. Qiu, *J. Phys. Chem. C* **2012**, *116*, 19451.
[28] H. Li, M. Hong, A. Scarpaci, X. He, C. Risko, J. S. Sears, S. Barlow, P. Winget, S. R. Marder, D. Kim, J.-L. Brédas, *Chem. Mater.* **2019**, *31*, 1507.
[29] F. Würthner, *Angew. Chem., Int. Ed.* **2020**, *59*, 14192.
[30] Z. He, C. Ke, B. Z. Tang, *ACS Omega* **2018**, *3*, 3267.
[31] S. Chen, C. Zhang, H. Xu, *Chem. Eng. J.* **2022**, *429*, 132327.
[32] C. Kirst, F. Zoller, T. Bräuniger, P. Mayer, D. Fattakhova-Rohlfing, K. Karaghiosoff, *Inorg. Chem.* **2021**, *60*, 2437.
[33] K. Groutchik, K. Jaiswal, R. Dobrovetsky, *Org. Biomol. Chem.* **2021**, *19*, 5544.
[34] L. Bergmann, J. Friedrichs, M. Mydlak, T. Baumann, M. Nieger, S. Bräse, *Chem. Commun.* **2013**, *49*, 6501.
[35] A. V. Artem'ev, M. R. Ryzhikov, I. V. Taidakov, M. I. Rakhmanova, E. A. Varaksina, I. Y. Bagryanskaya, S. F. Malysheva, N. A. Belogorlova, *Dalton Trans.* **2018**, *47*, 2701.
[36] A. V. Artem'ev, E. P. Doronina, M. I. Rakhmanova, A. O. Sutyrina, I. Y. Bagryanskaya, P. M. Tolstoy, A. L. Gushchin, A. S. Mazur, N. K. Gusarova, B. A. Trofimov, *New J. Chem.* **2016**, *40*, 10028.
[37] L. Douce, L. Charbonnière, M. Cesario, R. Ziessel, *New J. Chem.* **2001**, *25*, 1024.
[38] A. V. Artem'ev, A. Y. Baranov, M. I. Rakhmanova, S. F. Malysheva, D. G. Samsonenko, *New J. Chem.* **2020**, *44*, 6916.
[39] G. A. Bowmaker, J. V. Hanna, S. P. King, F. Marchetti, C. Pettinari, A. Pizzabiocca, B. W. Skelton, A. N. Sobolev, A. Tăbăcaru, A. H. White, *Eur. J. Inorg. Chem.* **2014**, *2014*, 6104.
[40] O. Crespo, M. C. Gimeno, A. Laguna, C. L. Larraz, *Z. Naturforsch.* **2009**, *64*, 1525.
[41] S. Bestgen, C. Schoo, B. L. Neumeier, T. J. Feuerstein, C. Zovko, R. Köppe, C. Feldmann, P. W. Roesky, *Angew. Chem., Int. Ed.* **2018**, *57*, 14265.
[42] I. M. Dixon, E. Lebon, P. Sutra, A. Igau, *Chem. Soc. Rev.* **2009**, *38*, 1621.
[43] M. I. Rogovoy, A. S. Berezin, D. G. Samsonenko, A. V. Artem'ev, *Inorg. Chem.* **2021**, *60*, 6680.
[44] A. Kermagoret, F. Tomicki, P. Braunstein, *Dalton Trans.* **2008**, *22*, 2945.
[45] T. Steiner, *Angew. Chem., Int. Ed.* **2002**, *41*, 48.
[46] M. A. Digman, V. R. Caiolfa, M. Zamai, E. Gratton, *Biophys. J.* **2008**, *94*, L14.
[47] G. I. Redford, R. M. Clegg, *J Fluoresc* **2005**, *15*, 805.
[48] W. Schrimpf, J. Jiang, Z. Ji, P. Hirschle, D. C. Lamb, O. M. Yaghi, S. Wuttke, *Nat. Commun.* **2018**, *9*, 1647.
[49] C. Kirst, N. A. Danaf, F. Knechtel, T. Arczynski, P. Mayer, D. C. Lamb, K. L. Karaghiosoff, *J. Mater. Chem. C* **2021**, *9*, 13366.
[50] M. A. Spackman, D. Jayatilaka, *CrystEngComm* **2009**, *11*, 19.
[51] P. R. Spackman, M. J. Turner, J. J. McKinnon, S. K. Wolff, D. J. Grimwood, D. Jayatilaka, M. A. Spackman, *J. Appl. Cryst.* **2021**, *54*, 1006.
[52] B. Kupcewicz, M. Małecka, *Cryst. Growth Des.* **2015**, *15*, 3893.
[53] R. Crespo-Otero, Q. Li, L. Blancafort, *Chem Asian J* **2019**, *14*, 700.
[54] J. Guan, R. Wei, A. Prlj, J. Peng, K.-H. Lin, J. Liu, H. Han, C. Corminboeuf, D. Zhao, Z. Yu, J. Zheng, *Angew. Chem., Int. Ed.* **2020**, *59*, 14903.
[55] Z. Zhao, H. Zhang, J. W. Y. Lam, B. Z. Tang, *Angew. Chem., Int. Ed.* **2020**, *59*, 14903.
[56] I. Linert, M. Zubek, *Eur. Phys. J. D* **2016**, *70*, 74.
[57] Z.-L. Cai, J. R. Reimers, *J. Phys. Chem. A* **2000**, *104*, 8389.
[58] I. Yamazaki, K. Sushida, H. Baba, *J. Chem. Phys.* **1979**, *71*, 381.